Chapter 3

BOLTZMANN TRANSPORT EQUATION

Chapter 3 has been adapted from:

(*1*) Chengyun Hua and Austin J. Minnich. "Analytical Green's function of the multidimensional frequency-dependent phonon Boltzmann equation". In: *Phys. Rev. B* 90 (21 2014), p. 214306. DOI: 10.1103/PhysRevB.90.214306. URL: http://link.aps.org/doi/10.1103/PhysRevB.90.214306.

(*2*) Chengyun Hua and Austin J. Minnich. "Semi-analytical solution to the frequency-dependent Boltzmann transport equation for cross-plane heat conduction in thin films". In: *Journal of Applied Physics* 117.17, 175306 (2015). DOI: http://dx.doi.org/10.1063/1.4919432. URL: http://scitation.aip.org/content/aip/journal/jap/117/17/10.1063/1.4919432.

3.1 Introduction

Heat conduction at length scale comparable to phonon wavelengths and mean free paths (MFPs) is of considerable interest recently(*33*) due to its applications in many technologies such as thermoelectrics(*10*, *12*) and electronic devices.(*34*) At these small scales, classic continuum transport theories such as Fourier's law are not valid due to the absence of scattering and therefore a local temperature.(*35*) In this non-diffusive regime, phonon transport is nonlocal and is described by the Boltzmann transport equation (BTE).(*21*)

Although numerical approaches such as the variance-reduced Monte Carlo methods introduced in Chapter 2 could efficiently solve the frequency-dependent BTE in a large, complex geometry with minimal memory requirements, analytical solutions to the BTE could enable physical insights to be obtained just from examining the form of the equation, which is not immediately accessible from the numerical so-

lutions. So far no analytical solutions to the BTE that could rigorously include the frequency dependence of thermal phonons have been reported.

Here, we report two analytical methods to solve the multidimensional, frequency-dependent transient BTE subject to different boundary conditions. Both methods allow us to obtain simple, closed-form solutions to complex multidimensional problems that have previously been possible to solve only with computationally expensive numerical simulations and will enable a better understanding of nondiffusive heat conduction.

3.2 Analytical Green's function of BTE

In this section, we demonstrate that exact analytical solutions to the multidimensional, frequency-dependent transient BTE for arbitrary heat inputs can be obtained using Fourier transforms in infinite or semi-infinite domains.

Derivation

The frequency-dependent BTE under relaxation time approximation is given by:

$$\frac{\partial g_\omega}{\partial t} + \mathbf{v}_g \cdot \nabla g_\omega - \frac{Q_\omega}{4\pi} = -\frac{g_\omega - g_0(T)}{\tau(\omega, T)}, \tag{3.1}$$

where $g_\omega = \hbar\omega D(\omega)(f_\omega(x,t,\theta) - f_0(T_0))$ is the desired deviational distribution function, $g_0(T)$ is the equilibrium deviational distribution function defined below, $Q_\omega(\mathbf{r},t)$ is the spectral volumetric heat generation, $\mathbf{v}_g(\omega,T)$ is the phonon group velocity, and $\tau(\omega,T)$ is the phonon relaxation time. Here, $\mathbf{r}$ is the spatial vector, t is the time, ω is the phonon frequency, and T is the temperature. In the Cartesian coordinate system and assuming an isotropical crystal, the advection term in Eq. (3.1) is expanded as

$$\mathbf{v}_g \cdot \nabla g_\omega = v_g \mu \frac{\partial g_\omega}{\partial z} + v_g \sqrt{1-\mu^2}\cos\phi \frac{\partial g_\omega}{\partial x} + v_g \sqrt{1-\mu^2}\sin\phi \frac{\partial g_\omega}{\partial y}, \tag{3.2}$$

where $\mu = cos(\theta)$ is the directional cosine of the polar angle θ and ϕ is the azimuthal angle. Here, we emphasize that while many crystals contain minor anisotropies in

the Brillouin zone, the vast majority of crystals are thermally isotropic, with notable exceptions being materials with very anisotropic bonding such as graphite. We present a validation of this assertion for the ab-initio calculations for silicon used here in Appendix C.

Assuming a small temperature rise, $\Delta T = T - T_0$, relative to a reference temperature, T_0, the equilibrium deviational distribution is proportional to ΔT,

$$g_0(T) = \frac{1}{4\pi}\hbar\omega D(\omega)(f_{BE}(T) - f_{BE}(T_0)) \approx \frac{1}{4\pi}C_\omega \Delta T. \tag{3.3}$$

Here, $\hbar$ is the reduced Planck constant, $D(\omega)$ is the phonon density of states, f_{BE} is the Bose-Einstein distribution, and $C_\omega = \hbar\omega D(\omega)\frac{\partial f_{BE}}{\partial T}$ is the mode specific heat. The volumetric heat capacity is then given by $C = \int_0^{\omega_m} C_\omega d\omega$ and the thermal conductivity $k = \int_0^{\omega_m} k_\omega d\omega$, where $k_\omega = \frac{1}{3}C_\omega v_\omega \Lambda_\omega$ and $\Lambda_\omega = \tau_\omega v_\omega$ is the phonon MFP.

Both g_ω and ΔT are unknown. Therefore to close the problem, we need to relate g_ω to ΔT. Notice that when intergrating over solid angle and phonon frequency, the left hand side of Eq. (3.1) becomes

$$\frac{\partial E}{\partial t} + \nabla \cdot \mathbf{q} - Q,$$

where $E = \int \int_0^{\omega_m} g_\omega d\omega d\Omega$ is the energy, $\mathbf{q} = \int \int_0^{\omega_m} \mathbf{v} g_\omega d\omega d\Omega$ is the heat flux, and $Q = \int \int_0^{\omega_m} Q_\omega d\omega d\Omega$ is the volumetric heat generation. This expression represents the general law of energy conversation and always equals to zero. Thefore, the energy conversation requires that the right hand side of Eq. (3.1) becomes

$$\int \int_0^{\omega_m} \left[\frac{g_\omega(\mathbf{r}, t)}{\tau_\omega} - \frac{1}{4\pi}\frac{C_\omega}{\tau_\omega}\Delta T(\mathbf{r}, t) \right] d\omega d\Omega = 0, \tag{3.4}$$

where Ω is the solid angle in spherical coordinates and ω_m is the cut-off frequency. Note that summation over phonon branches is implied without an explicit summation sign whenever an integration over phonon frequency is performed.

Let us now consider solving this equation in an infinite domain or a semi-infinite domain with specular boundary conditions such that the domain can be extended to infinity by symmetry. This assumption eliminates the consideration of diffuse boundaries but still leaves a wide range of problems that can be solved. In such a domain, a Fourier transform can be applied to all spatial coordinates as well as the time variable, giving:

$$(i\eta + v_g \mu i\xi_z + v_g \sqrt{1-\mu^2}\cos\phi i\xi_x + v_g \sqrt{1-\mu^2}\sin\phi i\xi_y)\widetilde{g}_\omega = -\frac{\widetilde{g}_\omega}{\tau_\omega} + \frac{C_\omega}{4\pi\tau_\omega}\Delta\widetilde{T} + \frac{\widetilde{Q}_\omega}{4\pi}, \tag{3.5}$$

where $\widetilde{\ }$ indicates the function is in its Fourier transform form. Here, we define the temporal frequency as η and the spatial wavevector in x, y and z as ξ_x, ξ_y, and ξ_z, respectively.

After rearranging Eq. (3.5), the unknown distribution function is written as

$$\widetilde{g}_\omega = \frac{C_\omega}{4\pi}\frac{\Delta\widetilde{T} + \widetilde{Q}_\omega\tau_\omega/C_\omega}{1 + i\eta\tau_\omega + i\mu\xi_z\Lambda_\omega + i\sqrt{1-\mu^2}(\cos\phi\xi_x\Lambda_\omega + \sin\phi\xi_y\Lambda_\omega)}. \tag{3.6}$$

Plugging Eq. (3.6) into Eq. (3.4), an equation for temperature can be obtained

$$4\pi\Delta\widetilde{T}\int_0^{\omega_m}\frac{C_\omega}{\tau_\omega}d\omega \tag{3.7}$$

$$= \int_0^{\omega_m}\int_0^{2\pi}\int_{-1}^{1}\frac{C_\omega}{\tau_\omega}\frac{\Delta\widetilde{T} + \widetilde{Q}_\omega\tau_\omega/C_\omega}{1 + i\eta\tau_\omega + i\mu\Lambda_\omega\xi_z + i\sqrt{1-\mu^2}(\cos\phi\xi_x\Lambda_\omega + \sin\phi\xi_y\Lambda_\omega)}d\mu d\phi d\omega.$$

The angle integrals on the right hand side of Eq. (3.7) can in fact be analytically evaluated using the identities 2.558-4 and 2.261 in Ref. (*87*). Therefore, a simple closed form of temperature in Fourier space can be obtained

$$\Delta\widetilde{T}(\eta,\xi_x,\xi_y,\xi_z) = \frac{\int_0^{\omega_m}\frac{\widetilde{Q}_\omega}{\Lambda_\omega\xi}\tan^{-1}\left(\frac{\Lambda_\omega\xi}{1+i\eta\tau_\omega}\right)d\omega}{\int_0^{\omega_m}\frac{C_\omega}{\tau_\omega}\left[1 - \frac{1}{\Lambda_\omega\xi}\tan^{-1}\left(\frac{\Lambda_\omega\xi}{1+i\eta\tau_\omega}\right)\right]d\omega}, \tag{3.8}$$

where $\xi = \sqrt{\xi_x^2 + \xi_y^2 + \xi_z^2}$. Note that if the spectral volumetric heat generation Q_ω is a Dirac-delta function in time and space, Eq. (3.8) becomes the impulse temperature response or the Green's function of the frequency dependent BTE. Once $\Delta\widetilde{T}$

is determined, $\widetilde{g_\omega}$ can be obtained by Eq. (3.6). The spectral heat flux is calculated as $\widetilde{\mathbf{q}}_\omega = \int \widetilde{g}_\omega v_g d^*$, thus closing the problem. Solutions to each of these quantities in the real-space solution can be easily obtained by inverse Fourier transform.

We next confirm that our solution reduces to the Green's function of the diffusive and ballistic regimes. These regimes can be specified by the two non-dimensional parameters, the Knudsen number $\mathrm{Kn}_\omega = \xi\Lambda_\omega$ and transient number $\Gamma_\omega = \eta\tau_\omega$ in Eq. (3.8). In the diffusive limit, length and time scales are much larger than the phonon MFPs and relaxation times, respectively, corresponding to $\mathrm{Kn}_\omega \ll 1$ and $\Gamma_\omega \ll 1$. Examining Eq. (3.8) under this limit, we find that in Eq. (3.8)

$$\frac{1}{\Lambda_\omega\xi}\tan^{-1}\left(\frac{\Lambda_\omega\xi}{1+i\eta\tau_\omega}\right) \sim 1 - i\eta\tau_\omega + \frac{1}{3}\Lambda_\omega^2\xi^2, \tag{3.9}$$

and the solution reduces to the Fourier solution, given by

$$\Delta\widetilde{T}_f \approx \frac{\widetilde{Q}_0}{i\eta C + \xi^2 k}, \tag{3.10}$$

where $\widetilde{Q}_0 = \int_0^{\omega_m} \widetilde{Q}_\omega d\omega$. In the ballistic regime, lengths and times are much smaller than MFPs and relaxation times, or $\mathrm{Kn}_\omega \gg 1$ and $\Gamma_\omega \gg 1$. The BTE thus becomes

$$\frac{\partial g_\omega}{\partial t} + \mathbf{v}_g \cdot \nabla g_\omega = 0, \tag{3.11}$$

the solution of which is the same as Eq. (3.8) under the limit of $\tau_\omega \to \infty$, given by

$$\Delta\widetilde{T}_b \approx \frac{1}{\int_0^{\omega_m} \frac{C_\omega}{\tau_\omega} d\omega} \int_0^{\omega_m} \frac{\widetilde{Q}_\omega}{\Lambda_\omega\xi}\tan^{-1}\left(\frac{v_\omega\xi}{i\eta}\right) d\omega. \tag{3.12}$$

Between these two limits is the quasiballistic regime for we must use the full expression given by Eq. (3.8).

Advantages of the method

The BTE has long been a formidable equation due to its high dimensionality and the efficient solution of this equation has been a long-standing challenge in the thermal sciences. Prior solution approaches in the thermal science literature are either

extremely simplified or solely numerical and usually computationally expensive. Independent of any numerical considerations, this identification of an analytical solution to BTE that enables physical insight to be obtained just from examining the form of the equation is a useful advance.

Further, the computational effort to obtain a solution for a specific problem is dramatically reduced as compared to that of discrete ordinates which have been typically used in the past. For example, the typical computational time for a problem with a heat impulse in a semi-infinite substrate using discrete ordinates(*79*) is on the order of five hours while our approach takes less than five seconds, a speedup exceeding three orders of magnitude. Furthermore, our result is valid for transient heat conduction in all three dimensions, a situation that has rarely been considered even numerically as the memory requirements for discrete ordinates in multiple dimensions are prohibitively large.

Applications

We now demonstrate the utility of our solution by solving three multidimensional problems for which the only previous solution methods were computationally expensive numerical approaches. We perform our calculations for crystalline silicon, using the density functional theory (DFT) dispersion and lifetimes calculated by J. Carrete and N. Mingo using ShengBTE (*88*, *89*) and Phonopy(*90*) from interatomic force constants obtained with VASP.(*91–94*) The details about converting the *ab initio* calculations to isotropic dispersion can be found in Appendix C.

The first case we consider here is the transient temperature decay of an infinite silicon crystal subject to a heat impulse with a Gaussian spatial profile. The spectral volume heat generation is given by:

$$Q_\omega(x, y, z, t) = \Delta T(0) C_\omega e^{-\pi \frac{x^2+y^2+z^2}{R^2}} \delta(t), \tag{3.13}$$

where R is the radius of the Gaussian profile as illustrated in the inset of Fig. 3.1. To

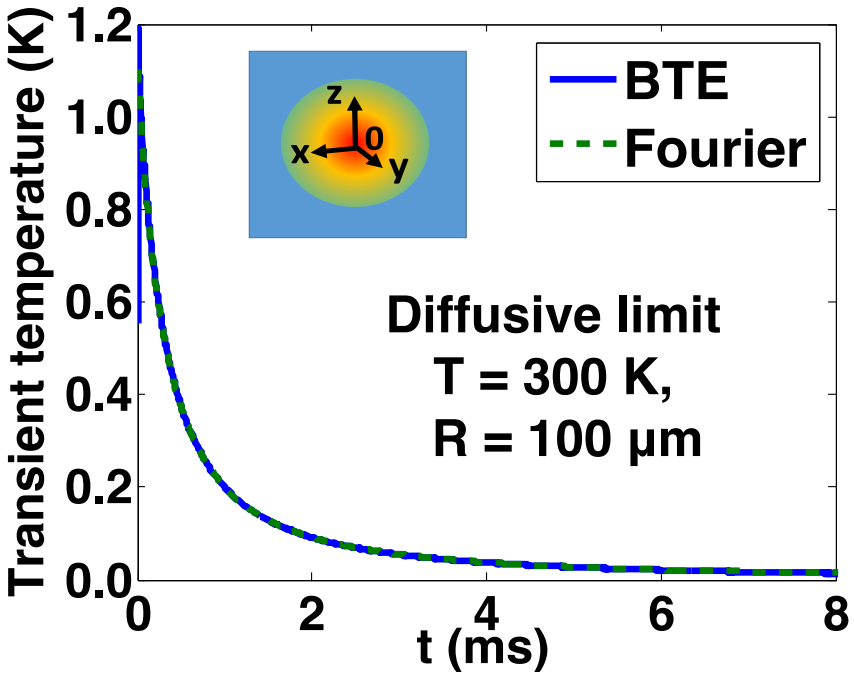

Figure 3.1: Temperature decay curves $\Delta T(t)$ at the origin for an infinite silicon sample subject to an impulsive volumetric heat generation with Gaussian spatial profile at the origin in the diffusive limit. The BTE and Fourier solutions are given by the solid lines and dashed lines respectively. Inset: 2D schematic of the domain. R is the Gaussian radius.

simplify the analytical expressions, we choose the amplitude of spectral distribution of heat generation to be $\Delta T(0)C_\omega$ corresponding to a thermal distribution. Note that this spectral distribution of heat generation can be varied according to the different circumstances.

After transforming Eq. (3.13) into Fourier space and inserting into Eq. (3.8), we obtain the temperature profile in Fourier space, given by

$$\Delta\widetilde{T}(\eta,\xi_x,\xi_y,\xi_z) = \Delta T(0)R^3 e^{-\frac{R^2\xi^2}{4\pi}} \frac{\int_0^{\omega_m} C_\omega \frac{1}{\Lambda_\omega \xi}\tan^{-1}\left(\frac{\Lambda_\omega \xi}{1+i\eta\tau_\omega}\right) d\omega}{\int_0^{\omega_m} \frac{C_\omega}{\tau_\omega}\left[1-\frac{1}{\Lambda_\omega \xi}\tan^{-1}\left(\frac{\Lambda_\omega \xi}{1+i\eta\tau_\omega}\right)\right] d\omega}. \tag{3.14}$$

Now, we examine how temperature decays with time at the origin. We note that to obtain this quantity it is not necessary to inverse Fourier transform the three spatial

wavevectors. Instead, we evaluate the Fourier transform only at $x = y = z = 0$ by integrating Eq. (3.8) over all wavevectors as

$$\Delta\widetilde{T}(\eta, \mathbf{r} = 0) = \frac{1}{(2\pi)^3} \int_{-\infty}^{\infty} \int_{-\infty}^{\infty} \int_{-\infty}^{\infty} \Delta\widetilde{T}(\eta, \xi_x, \xi_y, \xi_z) d\xi_x d\xi_y d\xi_z. \tag{3.15}$$

In this way, only one inverse Fourier transform over the frequency variable is required to obtain the temperature decay.

The resulting transient temperature decay curves are plotted in Figs. 3.1 & 3.2. In the diffusive limit where the heat generation region is big enough such that $\mathrm{Kn}_\omega \ll 1$ and $\Gamma_\omega \ll 1$, the BTE solution recovers the Fourier's law solution as in Fig. 3.1. As the Gaussian radius R decreases and MFPs become comparable or greater than R, we observe a deviation of the BTE solution from the Fourier's law due to quasiballistic transport, as shown in Fig. 3.2(a). We note that the actual temperature rise is larger than the Fourier's law prediction, consistent with a prior result by Chen.(*40*) The ballistic limit is plotted in Fig. 3.2(b), demonstrating that the calculated temperature decay agrees with the ballistic solution of the BTE given by Eq. (3.12).

The second case we consider is a line heater on a semi-infinite silicon substrate as illustrated in the inset of Fig. 3.3(a), where x is the in-plane direction and z is the cross-plane direction. The surface of the sample is subject to a periodic line heating with width L in the x direction, exponential decay with penetration depth δ in the z direction, and temporal frequency η. We assume that phonons at $z = 0$ are specularly reflected, leading to the adiabatic boundary condition $g_\omega(z = 0, x, t, \mu) = g_\omega(z = 0, x, t, -\mu)$. Therefore, by symmetry we can extend the domain to the negative z plane and apply our solution.

The spectral volumetric heat generation in this case is expressed as

$$Q_\omega(x, z, t) = \Delta T(0) C_\omega e^{i\eta t} e^{-|z|/\delta} \left[H\left(x + \frac{L}{2}\right) - H\left(x - \frac{L}{2}\right) \right], \tag{3.16}$$

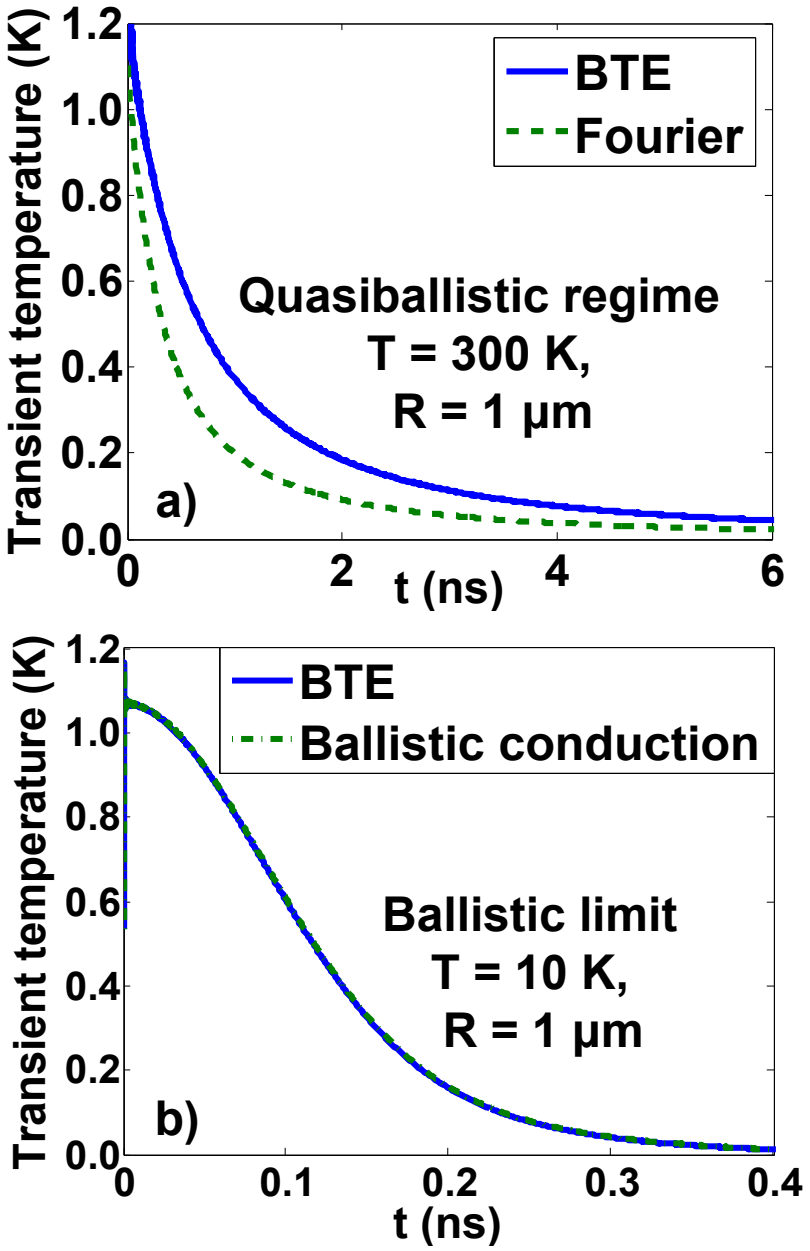

Figure 3.2: Temperature decay curves $\Delta T(t)$ at the origin for an infinite silicon sample subject to an impulsive volumetric heat generation with Gaussian spatial profile at the origin in (a) the quasiballistic regime and (b) the ballistic limit. The BTE, Fourier, and ballistic conduction solutions are given by the solid lines, dashed lines, and dash-dotted lines respectively.

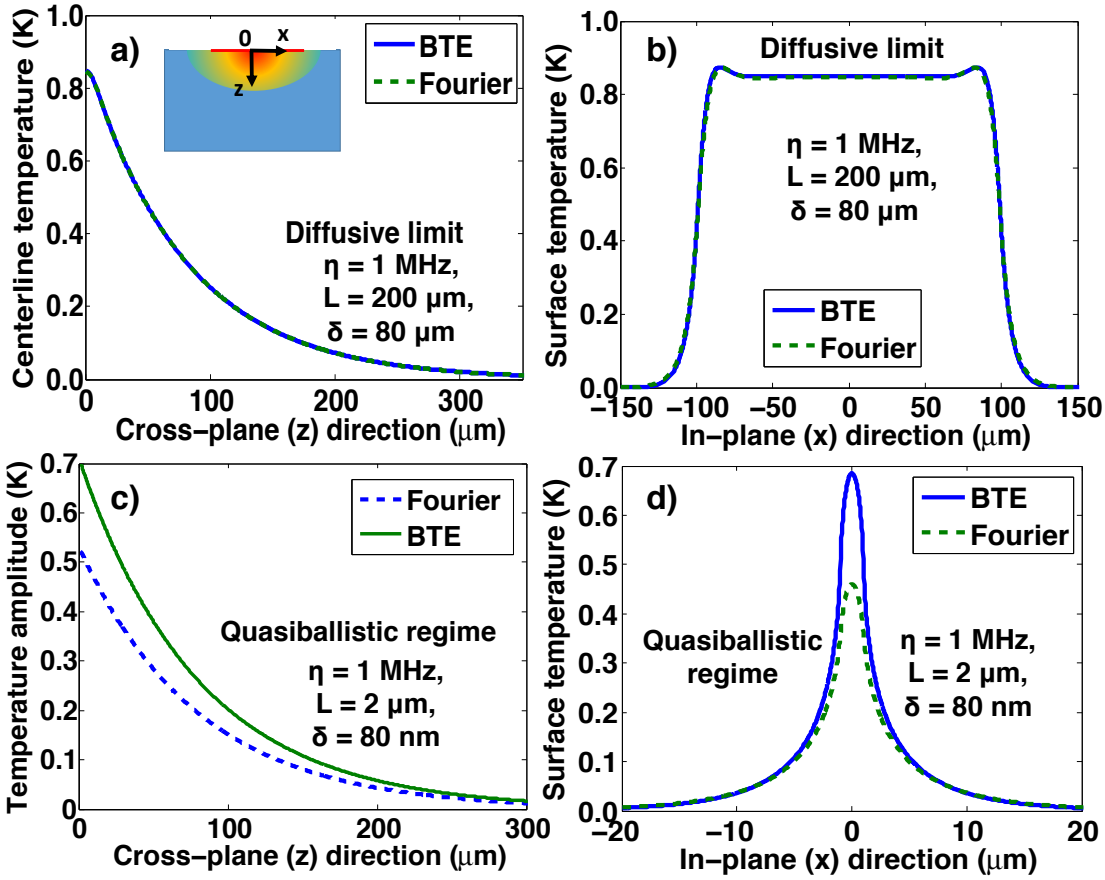

Figure 3.3: Amplitudes of the temperature decay curves $|\Delta T|$ for a planar semi-infinite silicon sample subject to a periodic line heater at the surface. ((a) & (b)) are in diffusive while ((c) & (d)) are in quasiballistic regime. The BTE and Fourier solutions are given by the solid and dashed lines, respectively. Inset in (a): 2D schematic of the geometry. Phonons incident on the plane at $z = 0$ are specularly reflected. The width of line heater is L with an exponential decay with penetration depth δ in the cross-plane direction, and η is the temporal frequency.

where H is the Heaviside step function. The same procedure as in the first case is carried out to obtain the temperature in Fourier space, which is given by

$$\Delta\widetilde{T}(\eta,\xi_x,\xi_y,\xi_z) = \Delta T(0)\frac{2\delta}{1+\delta^2\xi^2}L\text{sinc}\left(\frac{\xi_x L}{2}\right)\frac{\int_0^{\omega_m} C_\omega \frac{1}{\Lambda_\omega \xi}\tan^{-1}\left(\frac{\Lambda_\omega \xi}{1+i\eta\tau_\omega}\right)d\omega}{\int_0^{\omega_m}\frac{C_\omega}{\tau_\omega}\left[1-\frac{1}{\Lambda_\omega\xi}\tan^{-1}\left(\frac{\Lambda_\omega\xi}{1+i\eta\tau_\omega}\right)\right]d\omega}. \tag{3.17}$$

Since the heating is periodic in time, the temperature profile is quasi-stationary. We obtain the centerline temperature ($T(x = 0, z)$) by integrating Eq. (3.17) over all ξ_x and the surface temperature ($T(x, z = 0)$) by integrating Eq. (3.17) over all ξ_z.

The centerline temperature amplitudes are shown in Figs. 3.3 (a) & (b), and the surface temperature amplitudes are shown in Figs. 3.3 (b) & (d). Again, in the diffusive limit, the BTE solutions agree with the Fourier solutions when the heating length is much larger than the phonon MFPs such that $\mathrm{Kn}_\omega \ll 1$ and $\Gamma_\omega \ll 1$. The phonon transport becomes quasiballistic when the MFPs are comparable to or greater than the characteristic length scales in which case the BTE solutions no longer agree with the Fourier's law solutions. We again observe that the BTE solution predicts a higher temperature rise than the Fourier's law in the quasiballistic case due to a lack of scattering local to the heater.

The last case we consider here is a steady displaced planar Gaussian heating source next to an adiabatic specularly reflecting corner as illustrated in Fig. 3.4. While this geometry is complex, the problem can be effectively solved using the method of images as in elementary electrostatics.(*95*) To implement the method of images, we replace the specular boundaries with three identical heating sources located at the mirror locations across each symmetry plane. By symmetry and uniqueness of the solution for the linear BTE, this solution is equal to that of the original problem. The method of images is a general technique that can be easily applied to even more complex geometries than that considered here.

The spectral volumetric heat generation for the original and mirror heaters can be expressed as

$$Q_\omega(x, z, t) = \Delta T(0) C_\omega \left(f(x, z) + f(-x, -z) + f(x, -z) + f(-x, z) \right), \qquad (3.18)$$

where $f(x, z) = e^{-\pi \frac{(x-L)^2 + (z-L)^2}{R^2}}$, L is the displaced distance from the center of the heat to z/x axis, and R is the radius of the Gaussian profile.

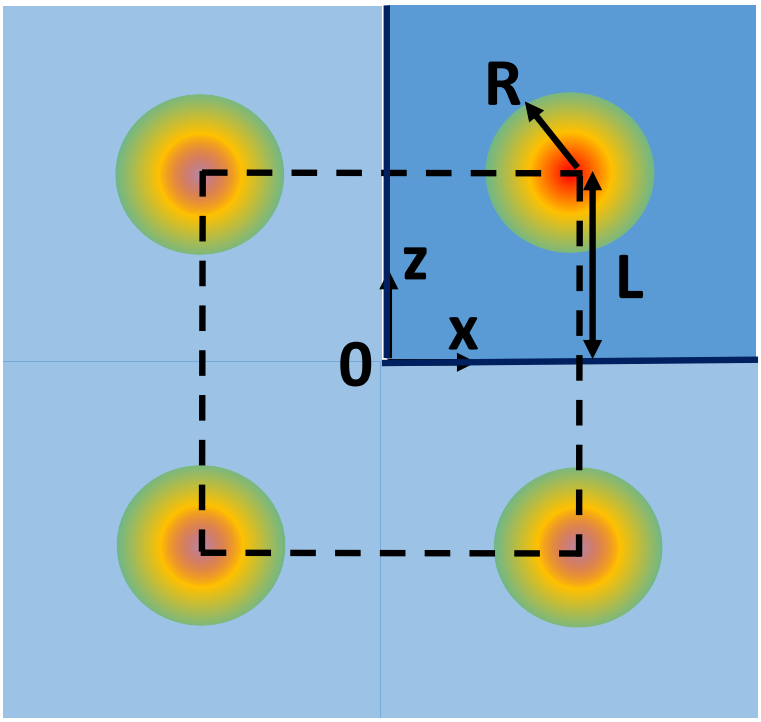

Figure 3.4: A planar domain located in the first quadrant subject to an Gaussian volumetric heat generation displaced away from the origin. The heating profile is uniform in the cross-plane direction. The radius of the Gaussian profile is R and the distance from the center of the heat to x/z axis is L. The problem is treated using the method of images in which the specular boundaries at $z = 0$ and $x = 0$ are replaced with three identical heating sources located at the mirror locations across each symmetry plane.

Figs. 3.5(a) & (b) give the amplitude of the temperature field when the heater is placed 10 μm away from both x and z axes based on the BTE and Fourier's law respectively. At the given the Gaussian radius ($R = 1$ μm), the phonon transport is quasiballistic. The peak amplitude of temperature predicted by the BTE is higher than that of Fourier's law. Also, due to a lack of scattering events local to the heater, heat is trapped around the heating source while it diffuses away from the heater by

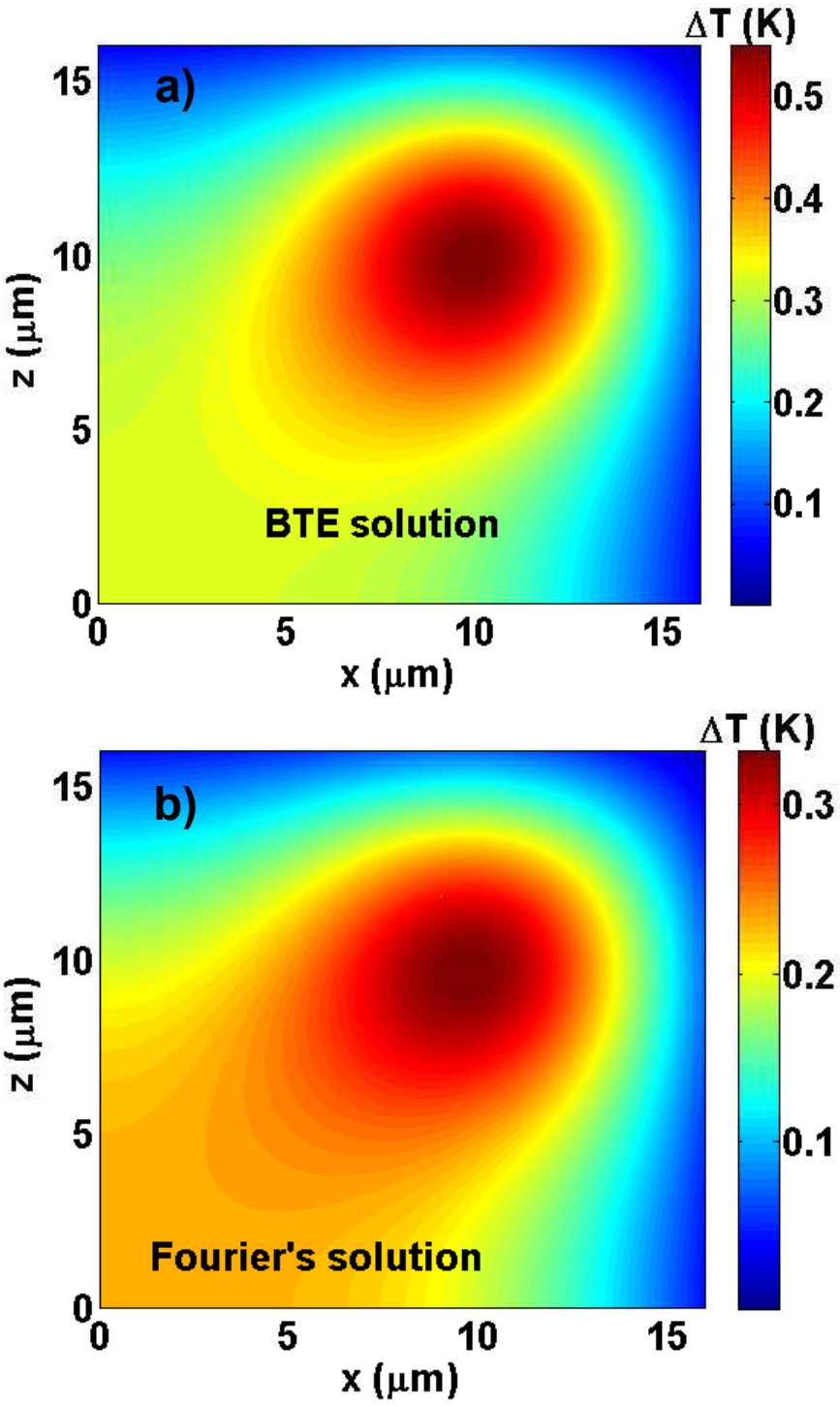

Figure 3.5: Amplitude of 2D temperature field $|\Delta T(x, z)|$ given by (a) the BTE and (b) Fourier's law in the quasiballistic regime with $L = 10\ \mu m$ and $R = 1\ \mu m$.

Fourier's prediction. In the past, the only method to solve this problem was purely numerical. Using our solution, we can write the exact solution in Fourier space, and we can obtain the real-space solution including frequency-dependent phonon properties in under one minute on a typical desktop computer.

3.3 BTE solutions in thin films

In this section, we consider crystals with finite thickness. In the past two decades, thermal transport in thin solid films with thicknesses from tens of nanometers to micrometers has become a topic of considerable importance.(*33*, *96–98*) Such films are used in applications ranging from quantum well lasers to electronic devices.(*99–101*) For example, boundary scattering in these films leads to reduced thermal conductivity that results in the inefficient removal of heat in GaN transistors and LEDs.(*8*, *102*, *103*) To address these and other problems, it is first necessary to understand the fundamental physics of heat conduction in micro-scale solid thin films.

Heat transport in thin films with thicknesses comparable to the phonon mean free paths (MFPs) is governed by the Boltzmann transport equation (BTE), which is an integro-differential equation of time, real space, and phase space. Due to its high dimensionality, it is in general very challenging to solve. For transport along the thin film, an analytical solution can be easily derived by assuming that the characteristic length scale of the thermal gradient is much longer than the phonon MFPs. Analytical solutions were derived for electron transport by Fuchs and Sondheimer with partially specular and partially diffuse boundary scattering.(*104*, *105*) Later, the Fuchs-Sondheimer solutions were extended to phonon thermal transport assuming an average phonon MFP, enabling the calculation of thermal conductivity as a function of the film thickness.(*106*, *107*) Mazumder and Majumdar used a Monte-Carlo method to study the phonon transport along a silicon thin film including phonon

dispersion and polarizations.(*108*)

Heat conduction perpendicular to the thin film (cross-plane direction) is much more challenging. In other fields such as neutron transport and thermal radiation, solutions to the BTE for a slab geometry have been obtained using an invariant embedding method,(*109*, *110*) an iterative method(*111*), and an eigenfunction expansion approach.(*112*) For heat conduction, Majumdar numerically solved the gray phonon Boltzmann transport using a discrete-ordinate method by assuming that the two surfaces of the film were black phonon emitters.(*35*) Later, Joshi and Majumdar developed an equation of phonon radiative transfer for both steady-state and transient cases, which showed the correct limiting behavior for both purely ballistic and diffusive transport.(*69*) Chen and Tien applied solutions from radiative heat transfer to calculate the thermal conductivity of a thin film attached to two thermal reservoirs.(*106*) Chen obtained approximate analytical solutions of the BTE to study ballistic phonon transport in the cross-plane direction of superlattices and addressed the inconsistent use of temperature definition at the interfaces.(*113*) Cross-plane heat conduction using a consistent temperature definition was then re-investigated by Chen and Zeng.(*114*, *115*)

Despite these extensive efforts to study transport in thin films based on the BTE, solutions for the cross-plane geometry are still only available with expensive numerical calculations. For example, no analogous Fuchs-Sondheimer formula for the in-plane thermal conductivity exists for the cross-plane direction. Furthermore, most of the previous approaches assumed a single phonon MFP even though recent work has demonstrated that the transport properties of phonons in solids vary widely over the broad thermal spectrum.(*63*, *70*) Incorporating frequency-dependent phonon properties with these prior numerical methods is extremely computationally expensive.

Here, we present a semi-analytical solution of the frequency-dependent transient BTE using the method of degenerate kernels, also known as a series expansion method.(*116*) Our approach is valid from the diffusive to ballistic transport regimes, is capable of incorporating a variety of boundary conditions, and is more than three orders of magnitude faster than prior numerical approaches. Further, we obtain a simple closed-form expression for cross-plane thermal conductivity, analogous to the Fuch-Sondheimer formula for the in-plane thermal conductivity, which enables the cross-plane thermal conductivity of a thin film to be easily calculated. Our results can be applied to efficiently solve heat conduction problems in numerous practical geometries such as superlattices and the thin films used in thermoreflectance experiments while rigorously incorporating the full phonon dispersion.

Method

We start with Eq. 3.1 and assume a small temperature rise, $\Delta T = T - T_0$, relative to a reference temperature, T_0. The one-dimensional (1D) frequency-dependent BTE for an isotropic crystal under the relaxation time approximation becomes:

$$\frac{\partial g_\omega}{\partial t} + v_g \mu \frac{\partial g_\omega}{\partial x} = -\frac{g_\omega}{\tau_\omega} + \frac{1}{4\pi}\frac{C_\omega}{\tau_\omega}\Delta T + \frac{Q_\omega}{4\pi}. \tag{3.19}$$

Again, to close the problem, energy conservation is used to relate g_ω to ΔT, given by

$$\int \int_0^{\omega_m} \left[\frac{g_\omega(x,t)}{\tau_\omega} - \frac{1}{4\pi}\frac{C_\omega}{\tau_\omega}\Delta T(x,t) \right] d\omega d\Omega = 0. \tag{3.20}$$

To solve this equation, we first transform it into an inhomogeneous first-order differential equation by applying a Fourier transform to the time variable, giving:

$$i\eta \widetilde{g_\omega} + v_g \mu \frac{d\widetilde{g_\omega}}{dx} = -\frac{\widetilde{g_\omega}}{\tau_\omega} + \frac{C_\omega}{\tau_\omega}\frac{\Delta \widetilde{T}}{4\pi} + \frac{\widetilde{Q_\omega}}{4\pi}, \tag{3.21}$$

where η is the temporal frequency. This equation has the general solution:

$$\widetilde{g_\omega^+}(x) = P_\omega e^{-\frac{\gamma_\omega}{\mu}x} + \int_0^x \frac{\Gamma(x')}{\mu} e^{\frac{\gamma_\omega}{\mu}(x'-x)} dx' \ (\mu \in (0,1]) \tag{3.22}$$

$$\widetilde{g_\omega^-}(x) = B_\omega e^{\frac{\gamma_\omega}{\mu}(L-x)} - \int_x^L \frac{\Gamma(x')}{\mu} e^{\frac{\gamma_\omega}{\mu}(x'-x)} dx' \ (\mu \in [-1,0]), \tag{3.23}$$

where $\Gamma(x') = \frac{C_\omega \Delta\widetilde{T}(x') + \widetilde{Q}_\omega(x')\tau_\omega}{4\pi\Lambda_\omega}$, $\gamma_\omega = (1 + i\eta\tau_\omega)/\Lambda_\omega$, L is the distance between the two walls, and P_ω and B_ω are the unknown coefficients determined by the boundary conditions. Here, $\widetilde{g^+}(x)$ indicates the forward-going phonons and $\widetilde{g^-}(x)$ the backward-going phonons. In this work, $\widetilde{g^+}(x)$ is specified at one of the two walls and $\widetilde{g^-}(x)$ is specified at the other.

Let us assume that the two boundaries are nonblack but diffuse with wall temperature ΔT_1 and ΔT_2, respectively. The boundary conditions can be written as:

$$\widetilde{g_\omega^+}(x=0) = P_\omega = \epsilon_1 \frac{C_\omega}{4\pi}\Delta T_1 + (1-\epsilon_1)\int_{-1}^0 \widetilde{g_\omega^-}(x=0,\mu)d\mu \tag{3.24}$$

$$\widetilde{g_\omega^-}(x=L) = B_\omega = \epsilon_2 \frac{C_\omega}{4\pi}\Delta T_2 + (1-\epsilon_2)\int_0^1 \widetilde{g_\omega^+}(x=L,\mu)d\mu, \tag{3.25}$$

where ϵ_1 and ϵ_2 are the emissivities of the hot and cold walls, respectively. When $\epsilon_1 = \epsilon_2 = 1$, the walls are black and we recover Dirichlet boundary conditions. Note that while we assume a thermal spectral distribution for the boundary condition, an arbitrary spectral profile can be specified by replacing the thermal distribution with the desired distribution. Equations (3.24) & (3.25) are specific for diffuse boundary scattering; the specular case is presented in Appendix A.

Applying the boundary conditions to Eqs. (5.6) & (5.7), we have

$$\begin{aligned}\widetilde{g_\omega^+}(x) &= A_{1\omega}\frac{C_\omega}{4\pi}e^{-\frac{\gamma_\omega}{\mu}x} + e^{-\frac{\gamma_\omega}{\mu}x}\int_0^L \Gamma(x')\left[D_\omega E_1(\gamma_\omega(L-x')) + B_{1\omega}E_1(\gamma_\omega x')\right]dx' \\ &+ \int_0^x \frac{\Gamma(x')}{\mu}e^{\frac{\gamma_\omega}{\mu}(x'-x)}dx' \ (\mu \in [0,1])\end{aligned} \tag{3.26}$$

$$\begin{aligned}\widetilde{g_\omega^-}(x) &= A_{2\omega}\frac{C_\omega}{4\pi}e^{-\frac{\gamma_\omega}{\mu}(L-x)} + e^{-\frac{\gamma_\omega}{\mu}(L-x)}\int_0^L \Gamma(x')\left[D_\omega E_1(\gamma_\omega x') + B_{2\omega}E_1(\gamma_\omega(L-x'))\right]dx' \\ &+ \int_x^L \frac{\Gamma(x')}{\mu}e^{-\frac{\gamma_\omega}{\mu}(x'-x)}dx' \ (\mu \in [0,1]),\end{aligned} \tag{3.27}$$

where

$$
\begin{aligned}
A_{1\omega} &= \frac{\epsilon_1\Delta T_1 + (1-\epsilon_1)\epsilon_2\Delta T_2 E_2(\gamma_\omega L)}{1-(1-\epsilon_1)(1-\epsilon_2)(E_2(\gamma_\omega L))^2},\ A_{2\omega} = \frac{\epsilon_2\Delta T_2 + (1-\epsilon_2)\epsilon_1\Delta T_1 E_2(\gamma_\omega L)}{1-(1-\epsilon_1)(1-\epsilon_2)(E_2(\gamma_\omega L))^2},\\
B_{1\omega} &= \frac{1-\epsilon_1}{1-(1-\epsilon_1)(1-\epsilon_2)(E_2(\gamma_\omega L))^2},\ B_{2\omega} = \frac{1-\epsilon_2}{1-(1-\epsilon_1)(1-\epsilon_2)(E_2(\gamma_\omega L))^2},\\
D_\omega &= \frac{(1-\epsilon_1)(1-\epsilon_2)E_2(\gamma_\omega L)}{1-(1-\epsilon_1)(1-\epsilon_2)(E_2(\gamma_\omega L))^2},
\end{aligned}
$$

and $E_n(x)$ is the exponential integral given by:(*21*)

$$
E_n(x) = \int_0^1 \mu^{n-2} e^{-\frac{x}{\mu}} d\mu. \tag{3.28}
$$

To close the problem, we plug Eqs. (3.26) & (3.27) into Eq. (5.4) and obtain an integral equation for temperature as:

$$
\begin{aligned}
2\int_0^{\omega_m} \frac{C_\omega}{\tau_\omega} d\omega \widetilde{\Delta T}(\widehat{x}) &= \int_0^{\omega_m} \frac{C_\omega}{\tau_\omega} \left[A_{1\omega}E_2\left(\widehat{\gamma}_\omega\widehat{x}\right) + A_{2\omega}E_2(\widehat{\gamma}_\omega(1-\widehat{x}))\right] d\omega\\
&+ \int_0^1\int_0^{\omega_m} \widetilde{Q}_\omega(x')\frac{G_\omega(\widehat{x},\widehat{x'})}{\mathrm{Kn}_\omega} d\omega d\widehat{x'}\\
&+ \int_0^1 \Delta\widetilde{T}(\widehat{x'})\int_0^{\omega_m} \frac{C_\omega G_\omega(\widehat{x},\widehat{x'})}{\mathrm{Kn}_\omega\tau_\omega} d\omega d\widehat{x'},
\end{aligned} \tag{3.29}
$$

where $\widehat{x} = x/L$, $\mathrm{Kn}_\omega = \Lambda_\omega/L$ is the Knudsen number, $\widehat{\gamma}_\omega = \frac{1+i\eta\tau_\omega}{\mathrm{Kn}_\omega}$ and

$$
\begin{aligned}
G_\omega(\widehat{x},\widehat{x'}) &= E_2(\widehat{\gamma}_\omega\widehat{x})\left[D_\omega E_1(\widehat{\gamma}_\omega(1-\widehat{x'})) + B_{1\omega}E_1(\widehat{\gamma}_\omega\widehat{x'})\right]\\
&+ E_2(\widehat{\gamma}_\omega(1-\widehat{x}))\left[D_\omega E_1(\widehat{\gamma}_\omega\widehat{x'}) + B_{1\omega}E_1(\widehat{\gamma}_\omega(1-\widehat{x'}))\right]\\
&+ E_1(\widehat{\gamma}_\omega|\widehat{x'}-\widehat{x}|).
\end{aligned} \tag{3.30}
$$

Equation (3.29) can be written in the form:

$$
\Delta T(\widehat{x}) = f(\widehat{x}) + \int_0^1 K(\widehat{x},\widehat{x'})\Delta T(\widehat{x'})d\widehat{x'}, \tag{3.31}
$$

where the kernel function $K(\widehat{x},\widehat{x'})$ is given by

$$
K(\widehat{x},\widehat{x'}) = \frac{1}{2\int_0^{\omega_m}\frac{C_\omega}{\tau_\omega}d\omega}\int_0^{\omega_m}\frac{C_\omega G_\omega(\widehat{x},\widehat{x'})}{\mathrm{Kn}_\omega\tau_\omega}d\omega \tag{3.32}
$$

and the inhomogeneous function $f(\widehat{x})$ is given by

$$f(\widehat{x}) = \frac{1}{2\int_0^{\omega_m} \frac{C_\omega}{\tau_\omega} d\omega} \int_0^{\omega_m} \frac{C_\omega}{\tau_\omega} \left[A_{1\omega} E_2(\widehat{\gamma}_\omega \widehat{x}) + A_{2\omega} E_2(\widehat{\gamma}_\omega (1-\widehat{x}))\right] d\omega + \frac{1}{2\int_0^{\omega_m} \frac{C_\omega}{\tau_\omega} d\omega} \int_0^1 \int_0^{\omega_m} \widetilde{Q}_\omega(x') \frac{G_\omega(\widehat{x}, \widehat{x}')}{\mathrm{Kn}_\omega} d\omega d\widehat{x}'. \quad (3.33)$$

From Eq. (3.31), we see that the governing equation is a Fredholm integral equation of the second kind. Previously, the gray version of Eq. (3.29) that assumes average phonon properties has been solved numerically using integral discretization method.(*21*) While this approach does yield the solution, it requires the filling and inversion of a large, dense matrix, an expensive calculation even for the gray case. Considering the full phonon dispersion adds additional integrations to calculate each element of the matrix, dramatically increasing the computational cost. Additionally, care must be taken to account for a singularity point at $\widehat{x}' = \widehat{x}$ since $E_1(0) \to \infty$.

Here, we solve this equation using the method of degenerate kernels,(*116*) which is much more efficient than the integral discretization method and automatically accounts for the singularity point at $\widehat{x}' = \widehat{x}$. This method is based on expanding all the functions in Eq. (3.31) in a Fourier series, then solving for the coefficients of the temperature profile. From the temperature $\Delta\widetilde{T}(\widehat{x})$, all other quantities such as the distribution and heat flux can be obtained.

To apply this method, we first need to expand the inhomogeneous function $f(\widehat{x})$ and kernel $K(\widehat{x}, \widehat{x}')$ with a Fourier series. This expansion is possible because both $f(\widehat{x})$ and $K(\widehat{x}, \widehat{x}')$ are continuous and continuously differentiable on the relevant spatial domains of normalized length between $[0, 1]$ and $[0, 1] \times [0, 1]$, respectively.(*116*) All the necessary functions can be expanded using a linear combination of sines and cosines; however, a substantial simplification can be obtained by solving a symmetric problem in which the spatial domain is extended to include its mirror

image by extending both $f(\widehat{x})$ and $K(\widehat{x},\widehat{x'})$ to [-1,1] and [-1,1] $\times$ [-1,1]. Because of the symmetry of this domain, all the coefficients for sine functions equal zero and the Fourier series for both functions reduces to a cosine expansion. $f(\widehat{x})$ is then approximated as

$$f_{(N)}(\widehat{x}) = \frac{1}{2}f_0 + \sum_{m=1}^{N} f_m \cos(m\pi\widehat{x}), \tag{3.34}$$

where $f_m = 2\int_0^1 f(\widehat{x})\cos(m\pi\widehat{x})d\widehat{x}$. The kernel $K(\widehat{x},\widehat{x'})$ can be represented by a degenerate double Fourier series, given by

$$\begin{aligned} K_{(N)}(\widehat{x},\widehat{x'}) = \frac{1}{4}k_{00} \quad &+ \quad \frac{1}{2}\sum_{m=1}^{N} k_{m0}\cos(m\pi\widehat{x}) + \frac{1}{2}\sum_{n=1}^{N} k_{0n}\cos(n\pi\widehat{x'}) \\ &+ \quad \sum_{m=1}^{N}\sum_{n=1}^{N} k_{mn}\cos(m\pi\widehat{x})\cos(n\pi\widehat{x'}), \end{aligned} \tag{3.35}$$

where

$$k_{mn} = 4\int_0^1\int_0^1 K(\widehat{x},\widehat{x'})\cos(m\pi\widehat{x})\cos(n\pi\widehat{x'})d\widehat{x}d\widehat{x'}. \tag{3.36}$$

Moreover, the convergence and completeness theorem of cosine functions guarantees that $K_{(N)}(\widehat{x},\widehat{x'})$ and $f_{(N)}(\widehat{x})$ converge to $K(\widehat{x},\widehat{x'})$ and $f(\widehat{x})$ as $N \to \infty$.(*117*)

Inserting Eqs. (3.34) & (3.35) into Eq. (3.31), we then obtain the following integral equation

$$\begin{aligned} \sum_{m=0}^{N} x_m\cos(m\pi\widehat{x}) \quad = \quad &\frac{1}{2}f_0 + \sum_{m=0}^{N} f_m\cos(m\pi\widehat{x}) + \int_0^1 \sum_{n=0}^{N} x_m\cos(n\pi\widehat{x'})\left[\frac{1}{4}k_{00}\right. \\ &+\frac{1}{2}\sum_{m=1}^{N} k_{m0}\cos(m\pi\widehat{x}) + \frac{1}{2}\sum_{n=1}^{N} k_{0n}\cos(n\pi\widehat{x'}) \\ &\left.+\sum_{m=1}^{N}\sum_{n=1}^{N} k_{mn}\cos(m\pi\widehat{x})\cos(n\pi\widehat{x'})\right] d\widehat{x'}, \end{aligned} \tag{3.37}$$

where x_m are the desired but unknown Fourier coefficients of $\Delta\widetilde{T}(\widehat{x})$.

Using the orthogonality of $\cos(n\pi\widehat{x})$ on [0, 1] gives a simpler form of Eq. (3.37):

$$\sum_{m=0}^{N} x_m\cos(m\pi\widehat{x}) = \frac{1}{2}f_0 + \sum_{m=0}^{N} f_m\cos(m\pi\widehat{x}) + \frac{1}{4}\sum_{m=0}^{N} k_{m0}x_m + \frac{1}{2}\sum_{m=1}^{N}\sum_{n=1}^{N} k_{mn}x_n\cos(m\pi\widehat{x}). \tag{3.38}$$

Grouping the terms with the same index m in cosine, a system of linear equations of x_m can be obtained as:

$$\bar{\bar{A}}\bar{x} = \bar{f}, \tag{3.39}$$

where $\bar{x}$ is the vector of unknown coefficient x_m and $\bar{f}$ is the vector of f_m in Eq. (3.34). The matrix $\bar{\bar{A}}$ contains elements $A_{00} = 1 - \frac{k_{00}}{4}$, $A_{0n} = -\frac{1}{2}k_{0n}$, $A_{n0} = -\frac{k_{n0}}{4}$, $A_{nn} = 1 - \frac{1}{2}k_{nn}$ and $A_{nm} = -\frac{1}{2}k_{nm}$ ($m \neq n \neq 0$). Expressions of the elements in $\bar{\bar{A}}$ can be obtained analytically for the specific kernel here and are given in Appendix B for the steady-state heat conduction with diffuse walls. Since there is no row or column in $\bar{\bar{A}}$ that is all zeros or a constant multiple of another row or column, it is always guaranteed that $\bar{\bar{A}}$ is non-singular and its inverse exists.

Solving the matrix system yields x_m and thus the temperature $\Delta\widetilde{T}(\widehat{x})$, $\widetilde{g_\omega^+}(x)$, and $\widetilde{g_\omega^-}(x)$ can be obtained from $\Delta\widetilde{T}(\widehat{x})$ using Eqs. (3.26) & (3.27). Finally, the spectral heat is given by:

$$q_\omega(x) = \int_{-1}^{1} g_\omega v_\omega \mu d\mu = \int_0^1 g_\omega^+ v_\omega \mu d\mu - \int_0^1 g_\omega^- v_\omega \mu d\mu, \tag{3.40}$$

thereby closing the problem.

Summary of the method

We now summarize the key steps to implement our method. The first step is to determine the appropriate boundary conditions for the problem and compute the constants in Eqs. (3.26) & (3.27). Subsequently, the kernel function $K(\widehat{x}, \widehat{x'})$ and the inhomogenous function $f(\widehat{x})$ can be obtained from Eq. (3.20), and their Fourier coefficients can be computed using Eqs. (3.34) & (3.35). The elements in $\bar{\bar{A}}$ correspond to the Fourier coefficients of kernel function $K(\widehat{x}, \widehat{x'})$, and $\bar{f}$ is a vector of the Fourier coefficients of the inhomogeneous part of Eq. (3.29). We emphasize that analytic expressions for all of these elements exist and can be obtained; examples of these coefficients for steady heat conduction with non-black, diffuse

boundaries are given in Appendix B. Once $\bar{\bar{A}}$ and $\bar{f}$ are obtained, Eq. (3.39) is solved by standard matrix methods to yield the coefficients x_m. Finally, $\Delta\widetilde{T}(\widehat{x})$ is given by $\sum_{m=0}^{N} x_m \cos(m\pi\widehat{x})$.

Efficiency of the method

The primary benefit of our method is the substantial reduction in computational cost compared to the widely used integral discretization approach. Since both $K_{(N)}(\widehat{x}, \widehat{x'})$ and $f_{(N)}(\widehat{x})$ converge to $K(\widehat{x}, \widehat{x'})$ and $f(\widehat{x})$ as $1/N^2$, only a few terms of expansion are required for accurate calculations. In practice, we find that only 20 terms are necessary before the calculation converges, meaning the required matrix is only 20×20. Compared to the traditional integral discretization method that requires a matrix on the order of 1000×1000 before convergence is achieved, our approach is at least 3 orders of magnitude faster. Further, as we will show in Section 3.3, our semi-analytical approach enables a closed-form solution for the cross-plane thermal conductivity of a thin film that is not possible to derive from the integral discretization method.

Demonstration of the method

As an example calculation, we consider steady-state heat conduction between two walls that are either black or non-black. In the former case, both wall emissivities ϵ_1 and ϵ_2 equal 1 while in the latter case they are set to 0.5. Assuming steady state and no heat generation inside the domain, $\eta = 0$, and $Q_\omega = 0$. The Fourier coefficients of $K(\widehat{x}, \widehat{x'})$ and $\bar{f}$ for these two specific cases are given in Appendix B. We perform our calculations for crystalline silicon, using the experimental dispersion in the [100] direction and assuming the crystals are isotropic. The numerical details concerning the dispersion and relaxation times are given in Ref. (*79*).

We calculate the deviational temperature distribution $\Delta T(\widehat{x})$ for different film thickness at different equilibrium temperatures as shown in Figs. 3.6 & 3.7 while keep-

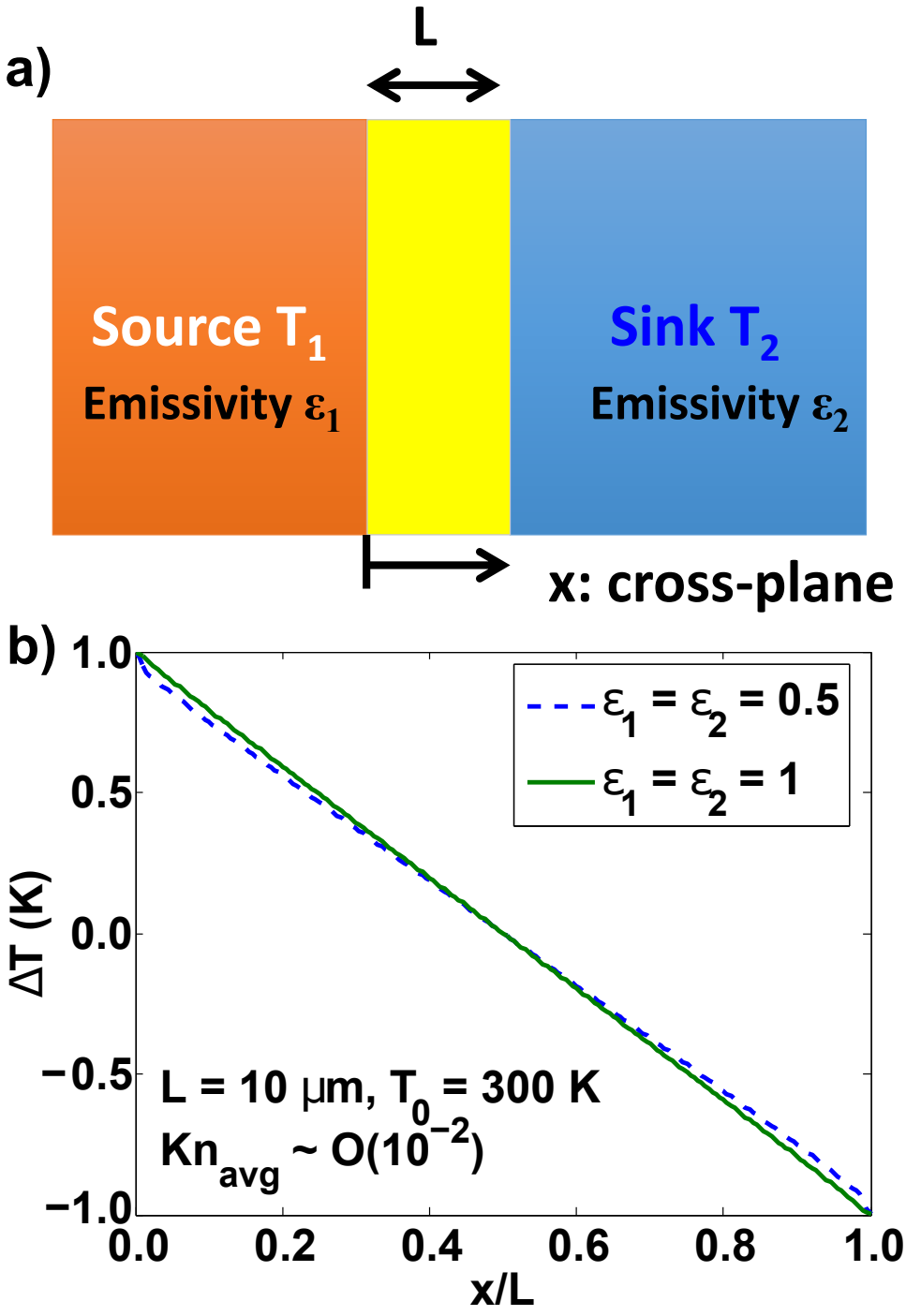

Figure 3.6: (a) Schematic of a planar slab with walls at different temperatures. (b)Temperature distribution $\Delta T(\widehat{x})$ for a planar slab with black walls (solid lines) and nonblack walls (dashed lines) when $\mathrm{Kn}_{avg} \sim O(10^{-2})$.

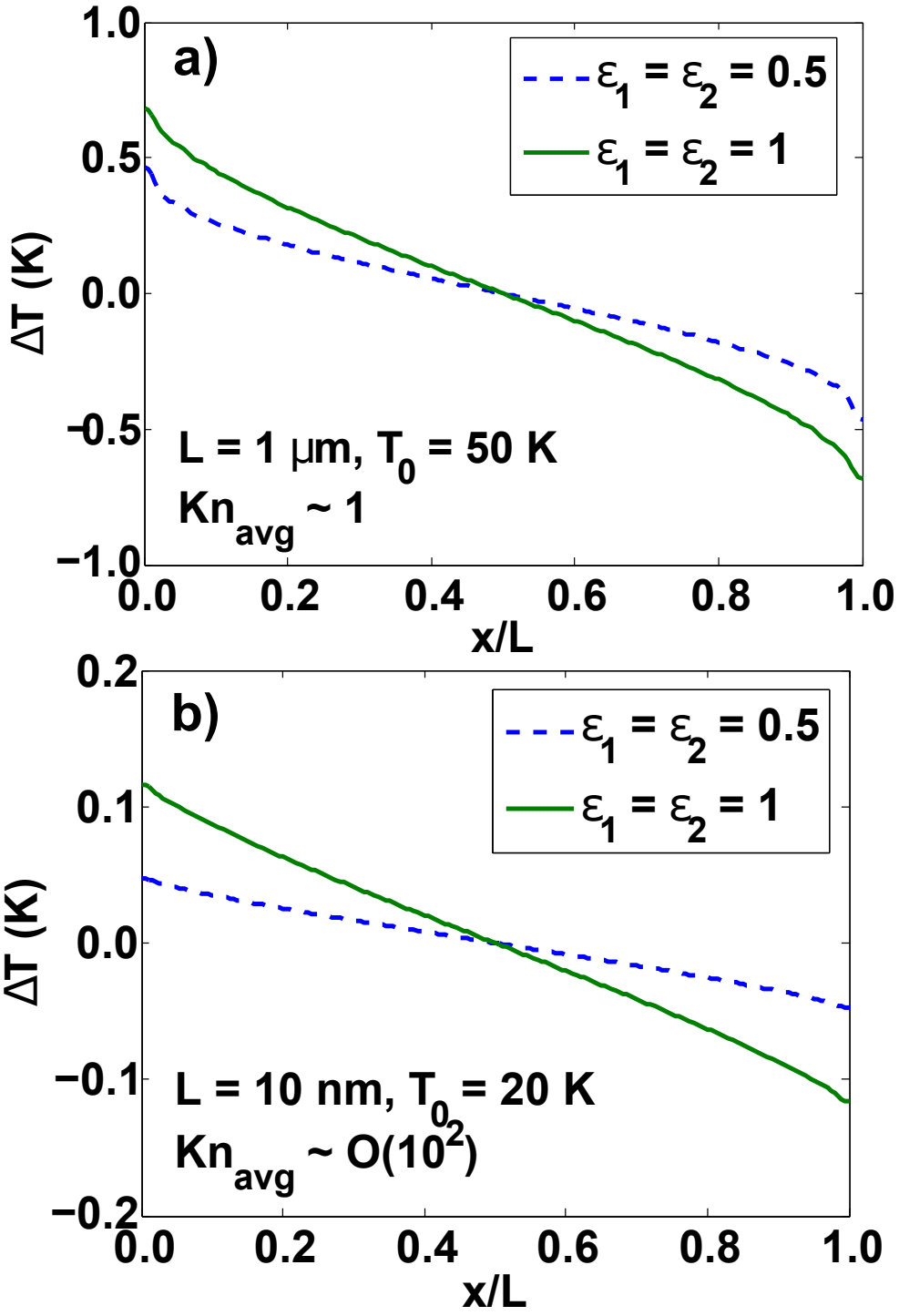

Figure 3.7: Temperature distribution $\Delta T(\widehat{x})$ for a planar slab with black walls (solid lines) and nonblack walls (dashed lines) when (a) $\mathrm{Kn}_{\mathrm{avg}} \sim 1$, and (b) $\mathrm{Kn}_{\mathrm{avg}} \sim O(10^2)$. As $\mathrm{Kn}_{\mathrm{avg}}$ increases, temperature slip at the boundaries grows larger.

ing $|\Delta T1| = |\Delta T_2| = 1$ K. When the averaged Knudsen number is small such that $\mathrm{Kn}_{avg} \ll 1$, the temperature profile remains linear. As thin film thickness decreases such that $\mathrm{Kn}_{avg} \sim 1$ or $\gg 1$, we observe a similar temperature slip as discussed in Ref. (*21*). These calculations take approximately one second to compute on a standard laptop computer. In contrast, the integral discretization method is at least 1000 times slower, requiring on the order of one hour to arrive at the same result.

In addition to the finite-layer geometry we consider above, the series expansion approach can be readily applied to many other thin film geometries, such as superlattices and the transducer film used in thermoreflectance experiments, by imposing different boundary conditions. Similar large reductions in computational cost can be expected for these cases.

Analytical formula for cross-plane thermal conductivity

Our semi-analytical approach also allows us to obtain a simple closed form expression for the cross-plane thermal conductivity as a function of film thickness, analogous to the Fuchs-Sondheimer expression for in-plane thermal conductivity. Such a formula allows the cross-plane thermal conductivity to be easily evaluated because the full solution of the BTE is no longer required. To derive this formula, we assume black walls and calculate the spatially averaged spectral heat flux that is integrated over the domain, defined as:

$$\int_0^1 q_\omega(\widehat{x})d\widehat{x} = \frac{1}{L}\int_0^L q_\omega(x)dx = \left(\frac{\Delta T_1 - \Delta T_2}{2}\right)\left[\frac{1}{3}C_\omega v_\omega \mathrm{Kn}_\omega - C_\omega v_\omega \mathrm{Kn}_\omega E_4\left(\frac{1}{\mathrm{Kn}_\omega}\right)\right]$$
$$+\frac{C_\omega v_\omega}{2\mathrm{Kn}_\omega}\left[\int_0^1\int_0^{\widehat{x}} \Delta T(\widehat{x}')E_2\left(\frac{|\widehat{x}' - \widehat{x}|}{\mathrm{Kn}_\omega}\right)d\widehat{x}'d\widehat{x} - \int_0^1\int_{\widehat{x}}^1 \Delta T(\widehat{x}')E_2\left(\frac{|\widehat{x}' - \widehat{x}|}{\mathrm{Kn}_\omega}\right)d\widehat{x}'d\widehat{x}\right] \tag{3.41}$$

Once x_m is solved from Eq. (3.37), we can insert the Fourier series of $\Delta T(x)$ into Eq. (3.41), which leads to

$$\begin{aligned}\int_0^1 q_\omega(\widehat{x})d\widehat{x} &= \left[\left(\frac{\Delta T_1 - \Delta T_2}{2}\right)\frac{1}{3}C_\omega v_\omega \mathrm{Kn}_\omega - C_\omega v_\omega \mathrm{Kn}_\omega E_4\left(\frac{1}{\mathrm{Kn}_\omega}\right)\right] \\ &+ \frac{C_\omega v_\omega}{2\mathrm{Kn}_\omega}\sum_{m=1}^{\infty} x_m[1-(-1)^m]\int_0^1 \frac{(\mathrm{Kn}_\omega\mu)^2\left(1+e^{-\frac{1}{\mathrm{Kn}_\omega\mu}}\right)}{1+(\mathrm{Kn}_\omega\mu)^2(m\pi)^2}d\mu.\end{aligned} \tag{3.42}$$

According to Fourier's law, the integrated heat flux is given by

$$\int_0^1 q_\omega^f(\widehat{x})d\widehat{x} = \frac{1}{3}C_\omega v_\omega \mathrm{Kn}_\omega(\Delta T_1 - \Delta T_2). \tag{3.43}$$

The heat suppression function is defined as the ratio of the BTE and Fourier's heat flux(*118*), given as

$$S(\mathrm{Kn}_\omega, L) = \frac{1}{2} - \frac{3}{2}E_4\left(\frac{1}{\mathrm{Kn}_\omega}\right) + \frac{3}{2}\sum_{m=1}^{\infty} x_m[1-(-1)^m]\int_0^1 \frac{\mu^2\left(1+e^{-\frac{1}{\mathrm{Kn}_\omega\mu}}\right)}{1+(\mathrm{Kn}_\omega\mu)^2(m\pi)^2}d\mu. \tag{3.44}$$

Note that the suppression function in general not only depends on Kn_ω but also is a function of geometry through x_m. The reduced or apparent thermal conductivity at a given domain thickness L is then given by:

$$k(L) = \int_0^{\omega_m}\frac{1}{3}C_\omega v_\omega \Lambda_\omega S(\mathrm{Kn}_\omega, L)d\omega. \tag{3.45}$$

This formula is analogous to the Fuch-Sondheimer equation for transport along thin films and allows the evaluation of the cross-plane thermal conductivity provided the expansion coefficients x_m are known. However, obtaining the expansion coefficients still requires solving the BTE as described above. A more useful result would be a suppression function that depends only on the Knudsen number as is available for in-plane heat conduction with the Fuchs-Sondheimer formula.(*104*, *105*)

To overcome this difficulty, we derive a simplified form of Eq. (3.44) that is valid under the conditions of most experiments. Note from Fig. 3.6(b) that for $\mathrm{Kn}_{avg} \sim$

$O(10^{-2})$, the temperature distribution is still linear, allowing us to simplify Eq. (3.44) by inserting the linear temperature distribution. Doing so leads to a simplified suppression function:

$$S_{\text{simplified}}(\text{Kn}_\omega) = 1 + 3\text{Kn}_\omega \left[E_5 \left(\frac{1}{\text{Kn}_\omega} \right) - \frac{1}{4} \right]. \tag{3.46}$$

This equation depends only on the Knudsen number and hence can be used to directly evaluate the cross-plane thermal conductivity given the phonon dispersion. This equation is valid provided that the ballistic modes are only low frequency phonons that contribute little to heat capacity, a situation that occurs often in experiment because high frequency phonons have short MFPs, on the order of tens of nanometers, at temperatures exceeding 20 K.

One important observation from Fig. 3.8(a) is that the exact and simplified suppression functions converge to the same curve at large Kn_ω. Also note that as the slab thickness decreases, the Knudsen number of a phonon with a particular MFP becomes larger. Therefore, in the limit of very small distance between the boundaries, the only important portion of the suppression function is at large values of Knudsen number exceeding $\text{Kn}_\omega = 1$ because phonons possess a finite minimum MFP. This observation suggests that for practical purposes the simplified suppression can be used even outside the range in which it is strictly valid with good accuracy. This simplification is very desirable because the simplified suppression function only depends on the Knudsen number and thus can be applied without any knowledge of other material properties.

Next, we apply this simplified suppression function to extract information about the phonon MPFs from the experimental measurements. In several works, thermal conductivity over variable lengths of nanostructures such as nanotubes, graphene ribbons and SiGe nanowires was measured. In principle, the measurements should contain information about MFPs: if phonons have MFPs exceeding the distance

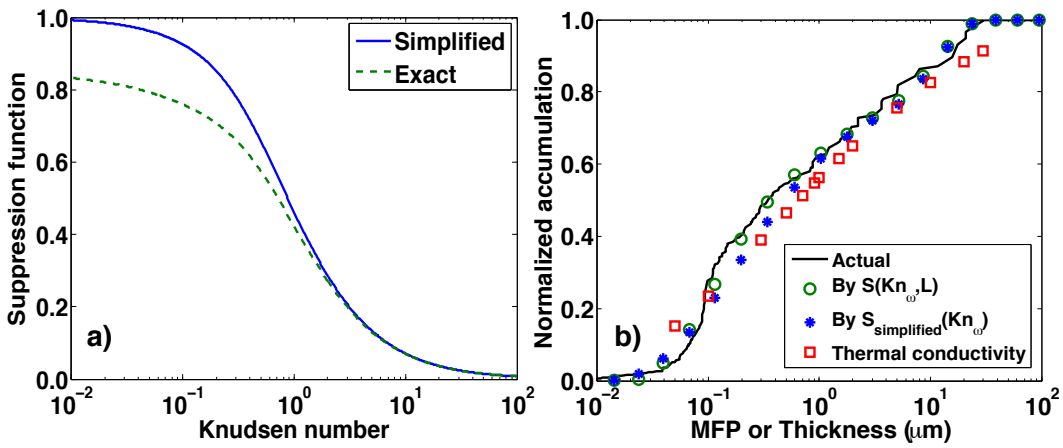

Figure 3.8: (a) Simplified (solid line) and exact (dashed line) suppression function versus Knudsen number. The exact and simplified suppression functions converge to the same curve at large Kn_ω. (b) Example MFP reconstructions for silicon at 300 K using numerically simulated data. Plotted are the analytical MFP distribution (solid line), the numerical apparent thermal conductivities (squares), and the reconstructed MFP distribution by the exact suppression function (circles) and by the simplified suppression function (stars). The x axis corresponds to the MFP for the distributions and to the slab thickness for the thermal conductivity data. Both the exact and simplified suppression functions yield satisfactory MFP reconstruction results.

between the heat source and the heat sink, their contribution to thermal conductivity is reduced compared to that in the bulk material, and thus the deviations of the measured thermal conductivity from the bulk value provide information on the phonon MFPs. Prior studies extracted only an average MFP despite the fact that recent works have demonstrated that in many solids phonon MFPs vary over orders of magnitude, make the approximation of an average MFP for all phonons quite poor.

The method proposed by Minnich is able to extract spectral MFP spectra from

variable-length thermal conductivity measurements by solving Eq. 3.45 as an inverse problem. The detailed description of the method is given in Ref. (*118*). Briefly, the variable-length thermal conductivities can be related to the MFP distribution $f(\Lambda_\omega)$ by

$$k_i = \int_0^\infty S(\mathrm{Kn}_\omega) f(\Lambda_\omega) d\Lambda_\omega, \tag{3.47}$$

where $S(\mathrm{Kn}_\omega)$ is the suppression function given by Eq. 3.44 or Eq. 3.46. If k_i's are known, $f(\Lambda_\omega)$ can be reconstructed using convex optimization.

To investigate the accuracy of Eq. 3.46, we perform the above reconstruction procedure to recover the MFP spectrum from thermal conductivity data as a function of slab thickness using both exact and simplified suppression functions. We synthesize effective thermal conductivities numerically using Eq. (3.45). Using these effective thermal conductivities and our knowledge of the suppression function, we use convex optimization to solve for the MFP spectrum. In the exact suppression function case, each slab thickness has its own suppression function given by Eq. (3.44) while in the simplified case Eq. (3.46) is used for all slab thicknesses.

As shown in Fig. 3.8(b), both the simplified and exact suppression functions yield satisfactory results. Even though the smallest thickness we consider here is 50 nm, close to the ballistic regime, the simplified suppression function still gives a decent prediction over the whole MFP spectrum, with a maximum of 15 % deviation from the actual MFP spectrum. For practical purposes, this deviation is comparable to uncertainties in experimental measurements and therefore the simplified suppression function can be used as an excellent approximation in the reconstruction procedure. This result demonstrates that length-dependent thermal conductivity measurements like those recently reported for SiGe nanowires(*119*) and graphene ribbons(*120*) can be used to reconstruct the full MFP spectrum rather than only an average MFP. We perform an investigation of our approach for this purpose in

Ref. (*121*).

3.4 Summary

In an infinite or semi-infinite domain, we have derived a new analytical Green's function of the multi-dimensional frequency-dependent BTE and demonstrated its capability to efficiently solve a wide range of problems that were previously intractable except using expensive numerical approaches. On the other hand, when the interested domain becomes finite, we have presented a series expansion method to solve the one-dimensional, transient frequency-dependent BTE and demonstrated its capability to describe cross-plane heat conduction in thin films. Our solution is valid from the diffusive to ballistic regimes, rigorously includes frequency dependence, and can be applied to a wide range of geometries.

With the time resolution on the order of tens of femtosecond from commercially available femtosecond laser sources and the spatial resolution on the order of tens of nanometers from nanoscale metallic heating structures, it becomes possible to directly access energy transport processes among phonons using ultrafast optical techniques. While ultrafast methods have shown their potential to probe the fundamental energy carriers, analysis of nanoscale energy transport occurring in those techniques remains challenging. With the BTE solutions we derived above, we are now able to accurately describe energy transport in some ultrafast optical experiments. In the next two chapter, we demonstrate how we are able to rigorously investigate the microscopic properties of thermal phonons using the unique combination of the ultrafast methods and BTE modeling.